Recent changes in air temperature, heat waves occurrences, and atmospheric circulation in Northern Africa.

Bernard Fontaine, Serge Janicot, Paul-Arthur Monerie

JOURNAL OF GEOPHYSICAL RESEARCH: ATMOSPHERES, VOL. 118, 8536–8552, doi:10.1002/jgrd.50667, 2013

Recent changes in air temperature, heat waves occurrences, and atmospheric circulation in Northern Africa

Bernard Fontaine,[1] Serge Janicot,[2] and Paul-Arthur Monerie[1]

Received 22 February 2013; revised 12 July 2013; accepted 18 July 2013; published 15 August 2013.

[1] This study documents the time evolution of air temperature and heat waves occurrences over Northern Africa for the period 1979–2011. A significant warming (1°–3°C), appearing by the mid-1960s over Sahara and Sahel, is associated with higher/lesser frequency of warm/cold temperatures, as with longer duration and higher occurrences of heat waves. Heat waves episodes of at least 4 day duration have been examined after removing the long-term evolution. These episodes are associated with specific anomalies: (i) in spring, positive low-level temperature anomalies over the Sahel and Sahara; low and midlevel cyclonic rotation over Morocco associated with a Rossby wave pattern, lessening the Harmattan; more/less atmospheric moisture westward/eastward to 0°; upward/downward anomalies above the western/eastern regions associated with the Rossby wave pattern; (ii) in summer, a similar but weaker positive low-level temperature anomaly (up to 3°C); less moisture westward to 10°W, a cyclonic anomaly in central Sahel favoring the monsoon eastward to 0° and a midlevel anticyclonic anomaly over the Western Sahara, increasing southward the flux divergence associated with the African Easterly Jet. In March–May, two to three heat waves propagate eastward. They are preceded by an abnormal warm cell over Libya and southwesterlies over the West Sahara. A large trough stands over North Atlantic while midtropospheric subsidence and anticyclonic rotation reinforce over the continent, then migrates toward the Arabian peninsula in breaking up. These signals are spatially coherent and might suggest the role of short Rossby waves with an eastward group velocity and a baroclinic mode, possibly associated with jet stream deformation.

Citation: Fontaine, B., S. Janicot, and P.-A. Monerie (2013), Recent changes in air temperature, heat waves occurrences, and atmospheric circulation in Northern Africa, *J. Geophys. Res. Atmos.*, *118*, 8536–8552, doi:10.1002/jgrd.50667.

1. Introduction

[2] The issue of climate warming in Africa has been particularly addressed through both empirical and numerical studies, showing that a high consensus exists on the reality of that warming over the continent. Thus, regarding the future, *Christensen et al*. [2007] evaluated the differences in near-surface temperature between the periods 2080–2099 and 1980–1999 in the multimodel of the AR4 experiment A1B projections, based on 21 atmosphere-ocean coupled models. The results show a temperature increase in all seasons with a median annual value of 3.3°C over West Africa with a maximum in March–May (3.5°C) and a minimum in December–February (3°C). They underline that such values are roughly 1.5 times the global mean response. The potential impact of that warming on extreme weather occurrences in the future is of course an important subject to study because long-term observations, registered along the last century as during the first decade of the 21st century, show that the frequency of temperature extremes increases globally [*Morak et al*., 2011].

[3] Regarding the African continent, the recent Special Report on extreme events of the Intergovernmental Panel on Climate Change [*IPCC*, 2012] indicates that there is low to medium confidence in observed trends in daily temperature extremes. It suggests an increase in hot extremes as in frequency of warm days and warm spells, and a decrease in cold extremes as in frequency of cold days and of cold nights, in western central Africa, Nigeria, and Gambia [*Alexander et al*., 2006; *New et al*., 2006; *Aguilar et al*., 2009; *Meehl et al*., 2009]. Such observations fit well with what is expected in a warmer climate and could be viewed as a regional consequence of the global warming induced by human activities: "it is likely that anthropogenic influences have led to warming of extreme daily minimum and maximum temperatures on the global scale" [*Seneviratne et al*., 2012].

[4] This article does not propose an attribution analysis of above features. It just explores statistically temperature and some associated circulation changes since the middle of the last century over northern Africa at both the monthly and daily time steps, using both observed and reanalyzed data sets. The study is threefold. Its first goal is to measure the magnitude of temperature evolution over the northern African continent over the seasons, regions, and periods

[1]Centre de Recherches de Climatologie, UMR Biogéosiences, CNRS/Université de Bourgogne, Dijon, France.
[2]IRD, LOCEAN/IPSL, UPMC, Paris, France.

Corresponding author: B. Fontaine, Centre de Recherches de Climatologie, UMR Biogéosiences, CNRS/Université de Bourgogne, F21000 Dijon, France. (fontaine@u-bourgogne.fr)

2169-897X/13/10.1002/jgrd.50667

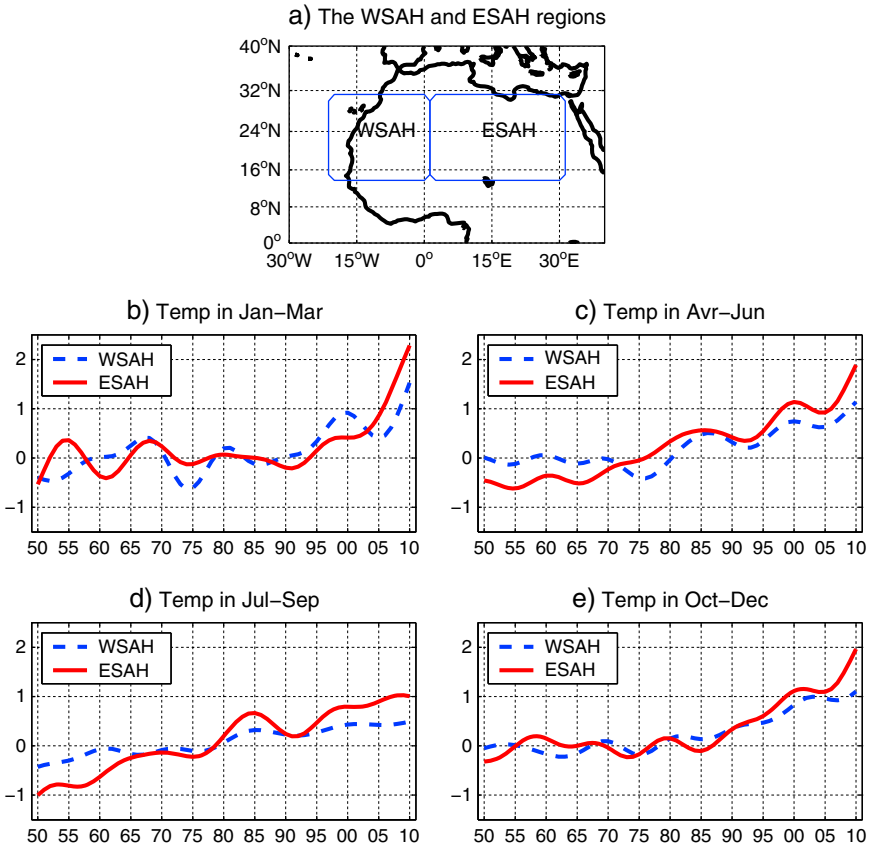

Figure 1. (a) Map of the WSAH and ESAH regions and (b–e) time evolution of mean near surface temperature anomalies from the mean 1961–1990 in degrees Celsius using the CRU data set averaged over the western and central-eastern Sahel for the (b) January–March, (c) April–June, (d) July–August, and (e) October–December (e) seasons: WSAH (10°N–25°N/20°W–0°); ESAH (10°N–25°N/0°–30°W) over the period 1950–2009.

which concentrate the most significant changes since the mid-20th century, through spatial indices and composite field differences. The second goal is to portray the evolution at the daily scale for the last 30 years — most concerned by the warming trend — in including the adjacent oceanic basins in terms of temperature and hot days and hot spell (heat wave) occurrences. The third aim is to define and discuss some significant circulation changes associated with thermal diagnostics through atmospheric variables.

2. Data and Method

[5] Because African regions, and in particular the sub-Saharan area, are insufficiently well sampled in terms of station observations and rawinsondes, most of the data used in this study come from analyzed data sets. Moreover, this choice will allow us to describe the thermal variability at regional and continental scales in consistency with spatial scales of atmospheric variability. The CRU TS 3.1 data set at a 0.5° resolution has been selected as the observational reference for estimating at the regional scale the evolution of continental air temperature near the surface over the period 1950–2009 at a monthly time step [*Mitchell and Jones*, 2005; *Harris et al.*, 2013]. To that aim two spatial indices are defined for documenting thermal changes by averaging the temperature over the westernmost (20°W–0°) and easternmost (0°–30°E) longitudes of a sub-Saharan zone extending from 10°N to 25°N. They will be, respectively, called the Western sub-Saharan (WSAH) and Eastern sub-Saharan (ESAH) indices (Figure 1a).

[6] Atmospheric data at finer space and time scales are added because thermal variability reflects both the internal variability of the climate system and external forcing through different mechanisms, e.g., change in the local energy balance and/or circulation changes [*Peterson et al.*, 2012] but also positive feedbacks between variables: since a warmer air contains more water vapor, the additional moisture could tend to intensify temperature extremes [*Santer et al.*, 2007; *Willett et al.*, 2007; *Arndt et al.*, 2010].

[7] Atmospheric data are not provided from synoptic resolution data sets because time series referring to individual stations at a subdaily or daily time scale exhibit too many gaps for computing heat wave occurrences and durations over the Saharan-Sahelian region, even when using the very recent HadISD data, a quality-controlled global synoptic report database for selected variables at long-term stations from 1973 to 2011[*Dunn et al.*, 2012]. Atmospheric data are provided from the NCEP/DOE AMIP-II Reanalysis (R-2) at a 2.5° resolution over the period 1979–2011. NCEP/DOE improves upon the NCEP/NCAR Reanalysis by updating the parameterizations of the physical processes and must be considered as a mix of in situ and satellite observations and modeling with updated

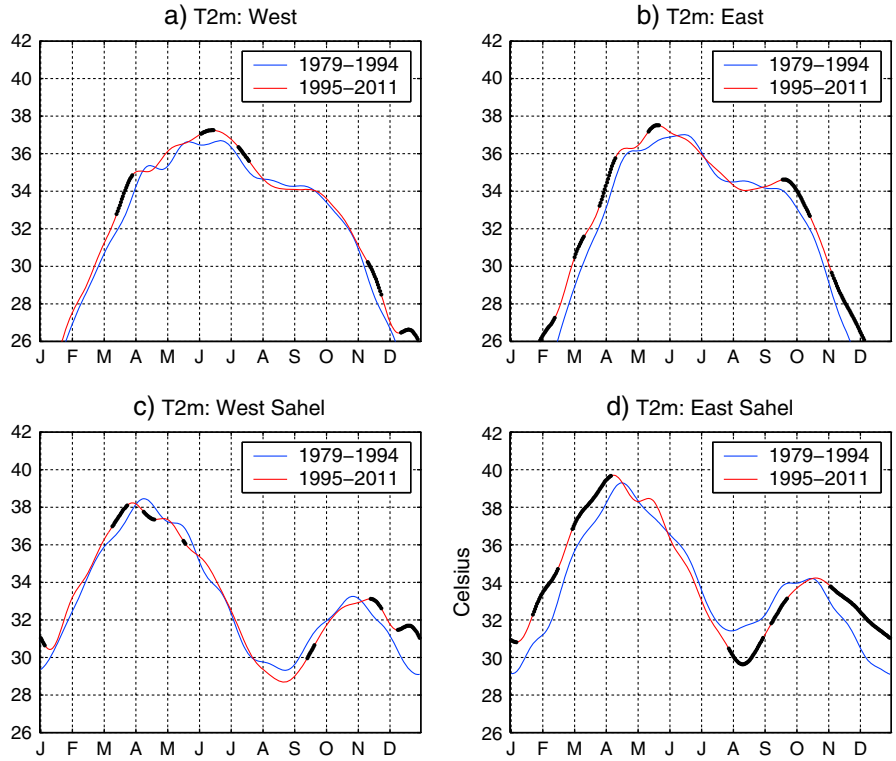

Figure 2. Daily temperature (T2m from NCEP2) differences between years 1995–2011 and 1979–1994, over the western (20°W–0°) and eastern (0°–30°W) West African regions: Figures 2a and 2b refer to the whole 10°N–25°N domain, while Figures 2c and 2d document the sole Sahelian belt between 10°N and 15°N. A 30 day filter has been applied for the display. The markers on the curves indicate the significant values regarding a Student's *t* test at p = 0.05.

representation of the boundary layer and convection schemes [*Kanamitsu et al*., 2002]. These data will allow us to better describe thermal changes in terms of frequency and intensity of extremes, and also to investigate their possible relationship with particular flow patterns. To this aim, we selected the daily averaged temperature and specific humidity at 2 m, the daily averaged Precipitable Water (PWT) for entire atmosphere, the omega vertical velocity (dP/dz) at 500 hPa (O500), along with the daily meridional (v-component) and zonal (u-component) wind components at 925 and 600 hPa (W925, W600).

[8] The daily averaged temperature at 2 m (T2m) has been chosen as a first approach because daily mean temperature is more representative of the daily atmospheric variability than maximum and minimum temperatures (TMIN, TMAX), especially for studying their relationship with the daily atmospheric variability. However, the minimum and maximum temperatures have been used in some sections and figures for better discussing the distribution of temperature extremes at the subdaily time scale. One should notice, however, that T2m, TMIN, and TMAX are classified in NCEP-NCAR reanalysis as B variables [*Kalnay et al*., 1996] meaning that they are influenced by both the observations and the model. Of course, regional temperature series derived from the NCEP DOE2 are sensitive to the availability of station data, but the satellite data are assimilated after 1979 which attenuates possible artificial jumps and trends, as shown by *Collins* [2011].

[9] In this study, the definitions of hot day occurrences, as of "heat waves" or "hot spells," take into account the particular thermal environment of the Northern African domain between 10°N and 25°N and are therefore different

Table 1. Monthly NCEP DOE2 (CRU) Near Surface Air Temperature Differences in Celsius Averaged Over the WSAH and ESAH Regions Between the Subperiods (1995–2010) and (1974–1994), Along With Correlation Values (CC*100) Between the Two Data Sets Over the Common Period 1979–2010[a]

		J	F	M	A	M	J	J	A	S	O	N	D
WSAH	NCEP	+0.8	+0.9*	+0.8*	+0.7*	+0.8*	+0.7*	+0.6*	+0.1	+0.2	+0.5	+0.7*	1.4*
	(CRU)	(+0.7*)	(+0.7*)	(+0.8*)	(+0.6*)	(+0.3)	(+0.4*)	(+0.3)	(+0.2)	(+0.3*)	(+0.3*)	(+0.7*)	(+1.0*)
	CC*100	+87	+80	+77	+81	+70	+60	+73	+67	+53	+55	+59	+90
ESAH	NCEP	+1.4*	+1.6*	+0.5	+0.9*	+0.5	+0.2	+0.2	+0.3	+0.6*	+1.4*	+1.3*	+1.8*
	(CRU)	(+1.0*)	(+0.9)	(+0.6)	(+0.9*)	(+0.7*)	(+0.3*)	(+0.7*)	(+0.4)	(+0.5*)	(+1.0*)	(+0.7)	(+1.3*)
	CC*100	+91	+89	+86	+88	+68	+53	+65	+67	+76	+91	+79	+75

[a]The significant differences regarding a Student's *t* test at p = 0.05 are indicated by an aster; all CCs are significant at p = 0.01 regarding a rank permutation test through Monte Carlo procedure.

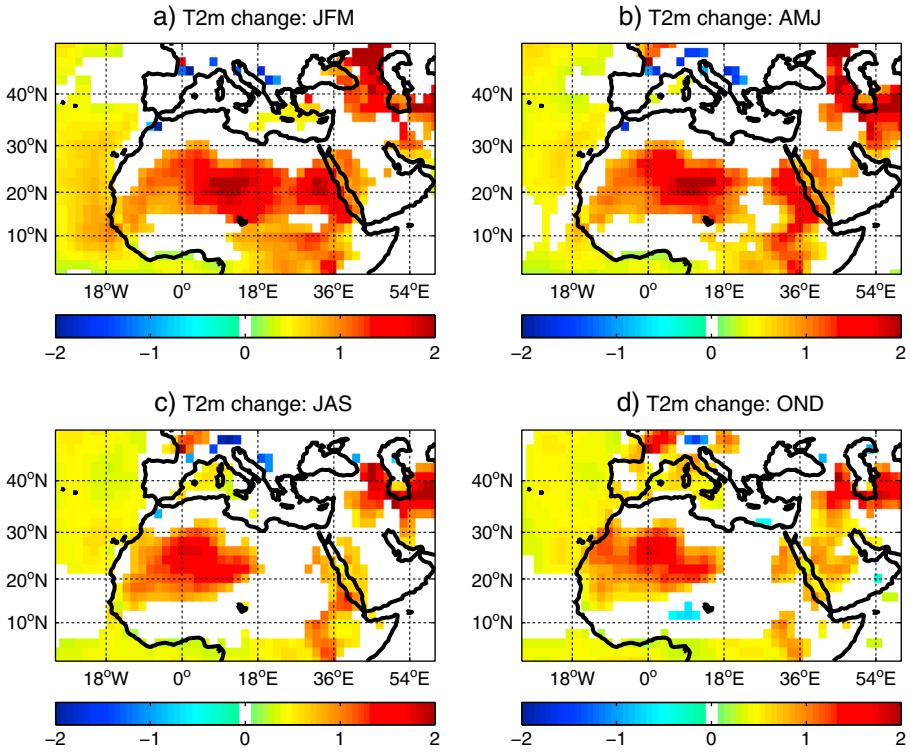

Figure 3. NCEP2 T2m differences (°C) between subperiods 1995–2009 and 1979–1994: (a) January–March, (b) April–June, (c) July–September, and (d) October–December. The significant signals regarding a Student's *t* test at the 95% confidence level are displayed.

from those usually proposed for analyzing crop and health impacts which are often based on station records and specific thresholds, depending on the population and country considered.

[10] Due to the range of sectors affected by heat waves, it is of course impossible to obtain a single index that can be calculated from readily available climatological data [*Perkins and Alexander*, 2012]. However, any heat wave is a period of consecutive days where conditions are excessively hotter than normal. In this study, hot days are defined from the NCEP/DOE AMIP-II Reanalysis data set when, for a given day, the daily temperature averaged over a few Sub-Saharan areas of interest exceeds the 90% percentile of daily variability, as estimated from the base period of historical data from the T2m values averaged over the same areas. This percentile optimizes the balance of "extreme" vs "measurable" events [*Perkins and Alexander*, 2012]. So, following the Expert Team on Climate Change Detection and Indices (ETCCDI) approach, the 90% percentile has been determined for each day using the temperature from that day and two days on either side of it, i.e., using successive 5 day moving windows over the whole period. In this context, the terms "heat waves" or "hot spells" consider consecutive days where the threshold is exceeded, i.e., when one observes hot days during several consecutive days inside a given area. We will focus in particular on heat wave durations equal or greater than 4 days because this threshold allows us to take into account the main heat events of synoptic scale occurring on the period. We will also examine the daily extreme TMIN and TMAX values but only through the 1979–2011 time series of heat wave occurrences (Figures 5 and 6) in order to discuss this evolution in more details.

[11] We analyze first the long-term evolution of temperature, hot days, and heat waves, taking into account the mean seasonal cycle, then we examine composite anomalies of these events independently to the long-term evolution.

3. Time Evolution

3.1. Air Surface Temperature

[12] Let us first observe the thermal trends over WSAH and ESAH, the two Sub-Saharan regions defined in section 2.

[13] Figure 1 displays the time evolution of seasonal temperature from 1950 to 2009 in January–March (winter; JFM), April–June (spring; AMJ), July–September (summer; JAS), and October–December (fall; OND) in terms of anomalies from the mean 1961–1990 using the CRU data set. Two comments can be made:

[14] 1. Overall, the warming is well observed over the two regions only since the 1990s in all seasons, and for the northern spring season since the mid-1960s over ESAH and the mid-1970s over WSAH (Figure 1c); before, in the 1950s, 1960s, and 1970s, it is not really attested in northern fall and winter, and only slightly during the summer rainy season.

[15] 2. The warming appears somewhat stronger eastward to the 0° longitude before the summer rainy season (+2.5°C in JFM and AMJ; 2°C in JAS), i.e., when maxima of solar radiation forcing are migrating northward. Notice also that, during the JAS rainy season, the trend is weaker due to the influence of rain amounts and higher cloudiness, which decreases air temperatures near the surface.

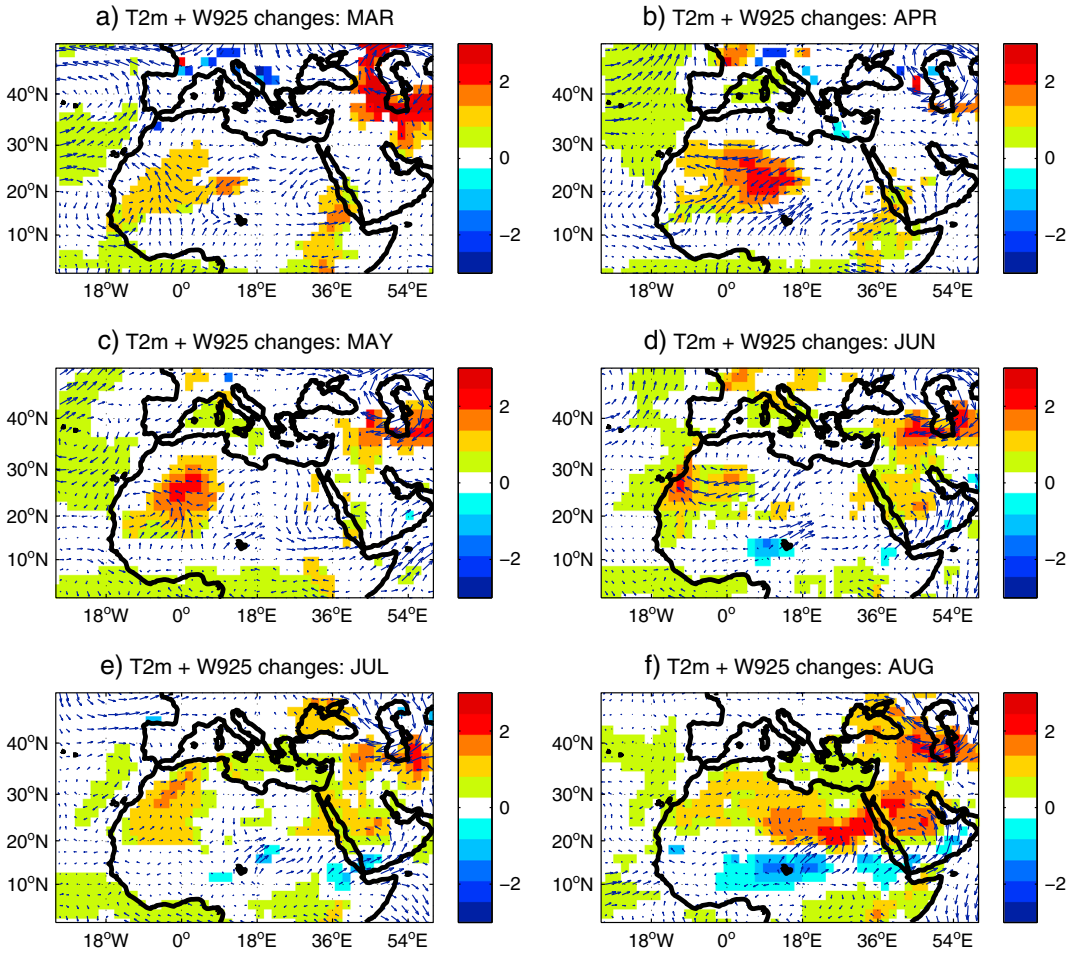

Figure 4. T2m and wind at 925 hPa differences in Celsius from March to August between subperiods 1995–2009 and 1979–1994. Only the values higher than 0.5°C and judged significant regarding a Student's *t* test at the 95% confidence level are shaded.

[16] The increasing positive trends after the mid-1990s mentioned in the first point are consistent with observations made by *Trenberth et al.* [2007] at global scale as with those relative to the sole African continent which demonstrate a significant rise in temperature between 1979 and 2010, with "more warming occurring in the most recent 10 years than the other periods examined" [*Collins*, 2011]. This could likely be related to aerosol effects such as the significant reduction in light-scattering anthropogenic sulfate aerosols after the 1980s (Reviewer's personal communication). However, as it will be pointed out in comments of Figures 5 and 6, the warming can be also viewed as a direct consequence of the greenhouse effect since it is more apparent at the end of the night than in diurnal maxima. Let us observe, however, that this warming in northern Africa is also concomitant with long-term SST evolution in the Northern Atlantic linked to the positive phase of the Atlantic Multidecadal Oscillation (AMO). Such a relationship is plausible since, as reported in the last IPCC Fourth Assessment Report: Climate Change 2007, a tropical multidecadal pattern related to the AMO exhibits coherent variations in tropical convection and surface temperatures in the West African monsoon region [*Chelliah and Bell*, 2004].

[17] The second point emphasizes the role of the primary natural forcing varying locally with the season. For this reason, the spring period is the most crucial, as illustrated in Figure 2 through the NCEP2 daily temperatures at T2m averaged over both regions for the subperiods 1979–1994 and 1995–2011. Notice first that when averaged between 10°N and 25°N, the T2m mean annual evolution exhibits a unimodal cycle peaking in northern spring due to the zenithal excursion although a secondary maximum can be observed in September over the ESAH area (Figure 2b): the thermal indices exceed 36°C in May over both regions (Figures 2a and 2b). By contrast air temperature decreases in summer in particular over ESAH, certainly as a response of rainfall processes (evaporation, cloud cover) occurring in summertime during the tropical rainy season: as illustrated in Figures 2c and 2d, this cooling is effectively attested between 10°N and 15°N in the Sahelian belt and explains also the fact that spring temperatures are warmer than those registered in fall within these latitudes.

[18] Second, the mean annual cycles computed over WSAH and ESAH show significant differences between the two subperiods, denoting the existence of a significant warming, as already shown with the CRU data in Figure 1. Over the last 33 years, the thermal increase is also more significant in winter, spring, and fall than during the rainy season in summer when a slight cooling takes place in August (Figures 2a and 2b) between 10°N and 25°N. However, it is noteworthy in Figure 2d that this cooling

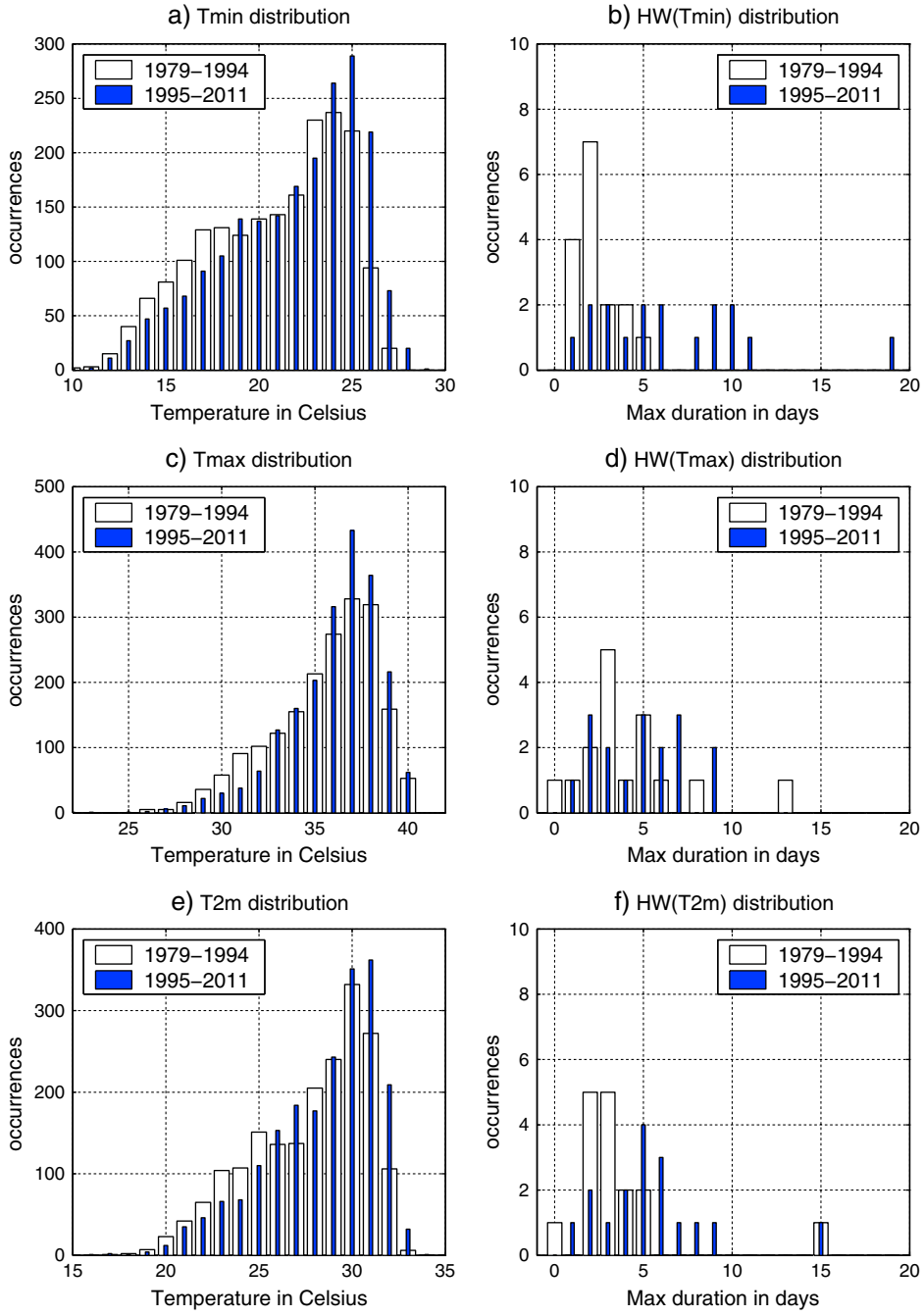

Figure 5. Histograms for the periods March–June 1979–1994 (large white bars) and 1995–2011 (thin blue bars). Left: daily temperature minima (a), maxima (c) and mean daily temperature at 2 m (T2m) in °C (c) averaged over the domain 10°N–25°N/10°W–10°E. Right: longest number of consecutive warm nights registered with minima (b), and longest heat waves registered with maxima (d) and T2m temperatures (f) according to the TN90p, TX90p, and T2m90p ETCCDI definitions.

reaches the statistical significance at $p = 0.05$ when averaged over the central-eastern Sahel region. This could be linked to the recent rainfall recovery observed at Sahelian latitudes [*Nicholson*, 2005; *Lebel and Ali*, 2009; *Fontaine et al.*, 2011a, 2011b], i.e., deficit of Solar energy input received during the day at the surface due to the extension of cloud coverage and intensification of evaporation processes.

[19] Table 1 allows us to better compare the recent thermal change at a monthly scale as a function of the data sets and over the common period 1979–2010. It is first noteworthy that between 10°N and 25°N, there is no strong discrepancy between the two data sources: temperature changes are rather similar and the correlation coefficients (CC*100 in Table 1) computed between the NCEP DOE2 and CRU series are all positive and significant at the 99% level, i.e., they vary from +0.53 to +0.91. Interestingly, the differences computed between the two subperiods are all positive and often significant at the 95% level: the values range from 0.1°C to 1.8°C

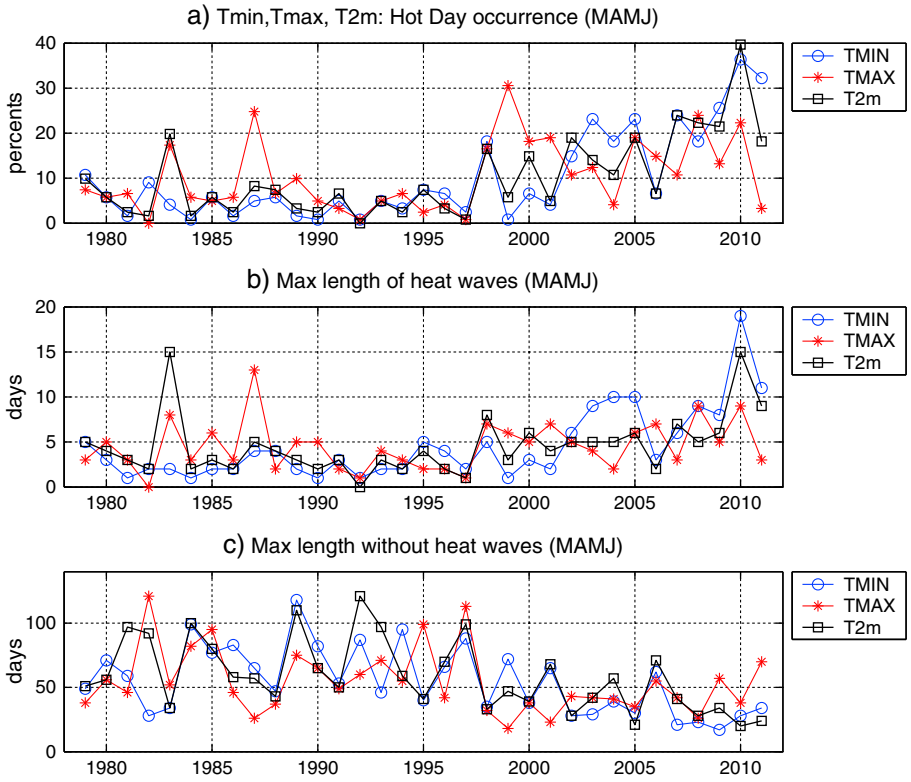

Figure 6. Time evolution of main statistics on hot day and heat waves using the NCEP2 daily air minimum (TMIN), maximum (TMAX), and daily (T2m) temperature at 2 m: (a) mean hot day frequencies in percents, using the TN90p and TX90P and T2m90p ETCCDI definitions; (b) length in days of the longer heat wave and (c) day interval maximum between 2 consecutive hot days. All statistics refer to March–June seasons during the period 1979–2011.

depending on the season: they are lower in northern summer during Sahelian rains, which confirms the results already displayed in Figures 1 and 2. We also examined the temperature trends over the Sahel and Sahara in some individual long-term station records available in data sets at monthly scale as in GCHN or at daily scale as in HadISD [*Dunn et al.*, 2012]. While a lot of gaps are present in these time series, a positive linear trend is clear (not shown).

3.2. Associated Spatial Patterns

[20] Let us focus now upon the NCEP DOE2 daily T2m temperature fields over the last 30 years in displaying the significant T2m differences registered between the periods 1995–2009 and 1979–1994.

[21] Figure 3 allows us to compare the spatial patterns of temperature differences registered at a seasonal time scale. The results confirm the existence of a significant warming in northern Africa. It is seen that T2m changes (Figures 3a–d) exhibit stronger signals over land (1.5°–2°C), mainly over the Arabian peninsula and the Sahara, with, however, some particularities for this latter region: the current warming is reinforced in winter and spring over the central desert but in summer and fall over the western part. The Atlantic and the Mediterranean Sea exhibit also positive thermal anomalies although of smaller magnitude, i.e., around 0.5°C, than on the continent. Thus, observations converge towards an intensification of the differential response between land and ocean, with stronger warming in the Sahara than in the Atlantic and Mediterranean. This tends to enhance, the ocean-land temperature gradients and therefore the flux convergence in low levels and the African monsoon circulation.

[22] Figure 4 displays similar composites but on a monthly basis from March to August and with the associated low-level wind changes. Over the continent T2m differences are more restricted over parts of the Sahara, just eastward to the Saharan Heat Low located over the western Sahara, between

Table 2. Composite Differences Between Daily Hot Occurrences and All Others for the Months From March to August Regarding the Precipitable Water Content in the Total Atmospheric Column (PWT in g/m^2) and the 2 m Specific Humidity (SHUM in g/m^2) Within the 25°N–17.5°N and 17.5°N–10°N Latitudinal Belts Inside the 10°W–10°E Longitudinal Window[a]

10°W–10°E		March	April	May	June	July	August
PWT	25°N–17.5°N	+2.8*	+1.2*	−0.2*	−0.7	−2.4*	−2.4*
	17.5°N–10°N	+2.9*	+1.1	−2.4*	−2.0*	−2.7*	−2.5*
SHUM	25°N–17.5°N	+0.8*	+0.4*	+0.11	−0.24*	0	−0.3*
	17.5°N–10°N	+1.1*	+0.6*	+0.3*	−0.5*	−0.8*	−1.2*

[a]The significant differences regarding a Student's *t* test at the 95% confidence level are marked by an aster.

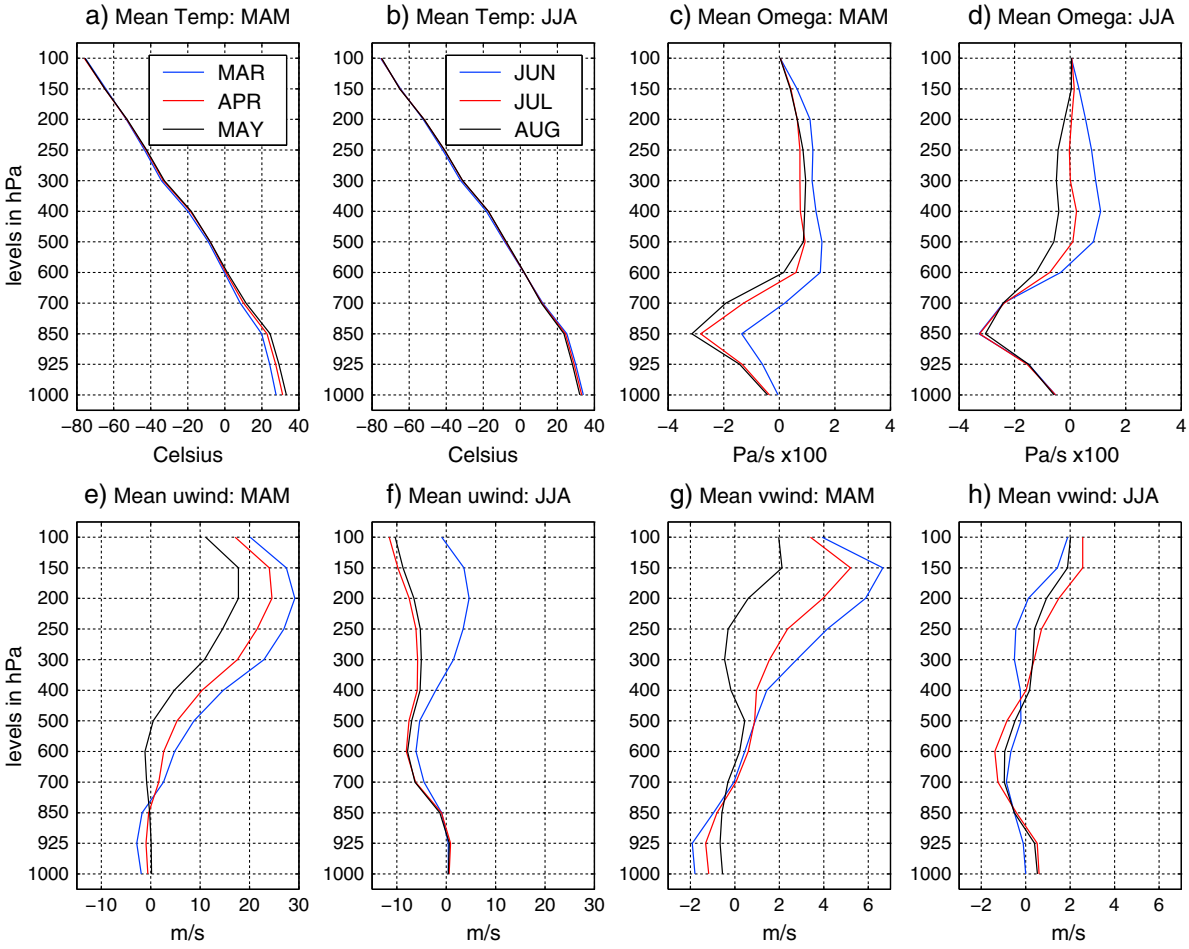

Figure 7. Mean vertical profiles of some basic daily tropospheric variables (1000 hPa to 100 hPa) averaged over the central WAM area (10°N–25°/10°W–10°E) for the months from March to August (1979–2009): (a–b) Air temperature at 2 m (c–d) omega vertical velocity in Pa/s x100; (e–f) zonal wind component in m/s and (g–h) meridional wind component in m/s.

the Hoggar and the Atlas mountains in northern summer [*Lavaysse et al.*, 2009]: here the warming can be estimated in the range of 1°–3°C in April (Figure 4b), and from March to May, it is associated with a cyclonic vorticity anomaly over the western Sahara, as shown by the counter-clockwise cells in Figures 4a–c. By contrast, from June to August (Figures 4d–f), the warming extends toward the eastern Saharan and Arabian deserts while a cooling and southwesterly anomalies, possibly linked to the recent rainfall recovery, appear southward (10°N–15°N) in central Sahel, in particular at the peak of the rainy season in August (Figure 4f). We can also notice a slighter warming over the eastern Atlantic and the Mediterranean Sea (over the western basin from April to June and over the eastern basin in July and August).

3.3. Hot Day, Heat Wave Occurrences, and Vertical Profiles

[23] Histograms of the daily TMIN, TMAX, and T2m temperatures at 2 m and of the longest durations of heat waves in days registered from March to June for the periods 1979–1994 and 1995–2011 are now presented in Figure 5 according to the ETCCDI approach. The values are relative to the domain 10°N–25°N/10°W–10°E which concentrates most of the significant temperature changes seen in Figure 3. Overall, one observes higher (lesser) frequencies of both warm (cold) temperatures and longer (shorter) heat wave durations after the year 1994, as attested by the rightward shifts of intervals (thin bars in blue in Figures 5a–d). It is noteworthy that changes in TMIN, TMAX, and T2m statistical distributions are significant at $p = 0.05$ regarding a two-sample Kolmogorov-Smirnov test. This is also verified with the number of consecutive warm nights defined from TMIN and with the length of heat wave defined from T2m. The most recent period shows in particular: (i) lower occurrences of TMIN below 19°C, of TMAX below 33°C and of T2m below 26°C, (ii) higher occurrences of TMIN above 24°C, of TMAX above 35°C and of T2m above 28°C (Figures 5a, 5c, and 5e), and (iii) longer TMIN and T2m heat waves, as shown in Figures 5b and 5f.

[24] Time evolution statistics of hot days and heat waves are presented in Figure 6 for the region 10°N–25°N/10W–10E concentrating most of the significant temperature changes seen previously. We focus on months from March to June that have the highest temperatures (Figure 2). The upper diagram (Figure 6a) shows that, except during the warm ENSO episodes of 1983 and 1987, hot events frequencies, especially those registered with TMIN and T2m, are clearly increasing

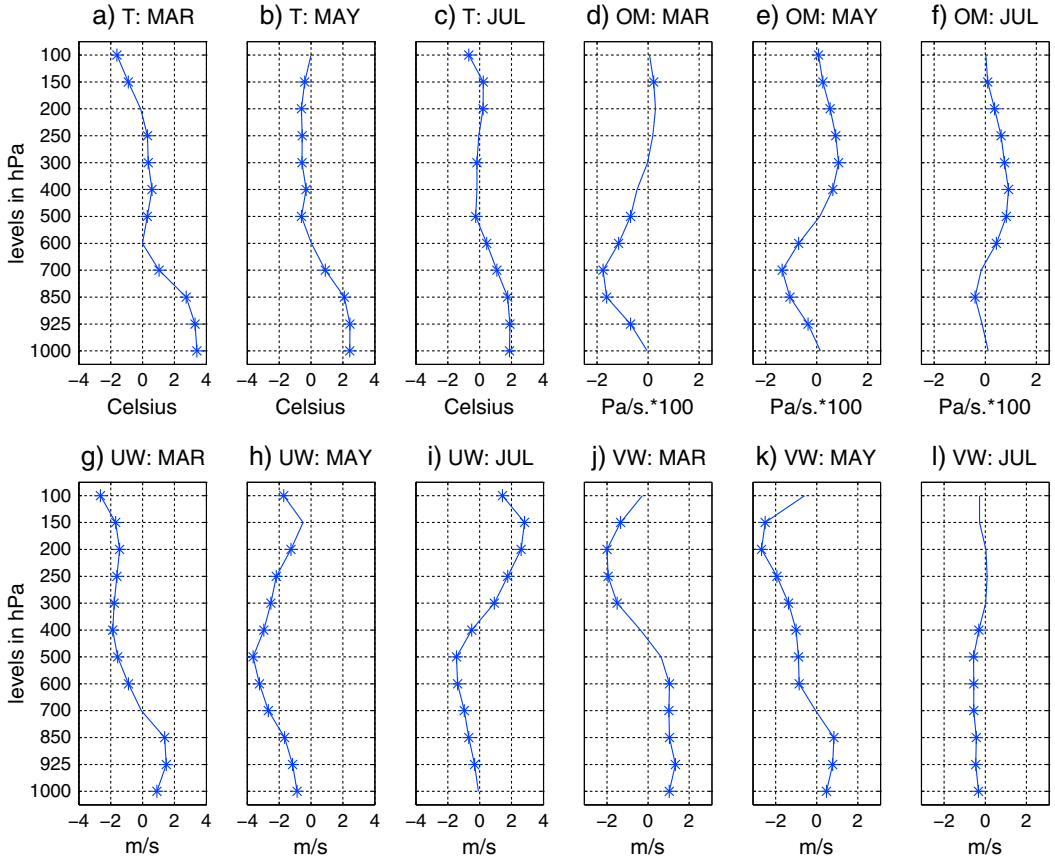

Figure 8. Composite differences between daily hot occurrences and all others along the vertical. The significant differences regarding a Student's *t* test at the 95% confidence level are marked by an aster.

after 1997, with a mean frequency multiplied by 2 or 3. One observes clearly a longer duration of heat waves in last years (Figure 6b). Notice also that heat waves occurring before 1998 are often shorter than 5 days, whereas they are frequently above this threshold after (Figure 6b). Another associated feature is the shorter day intervals between two consecutive hot events defined as the period without any hot occurrence (Figure 6c). Overall, and as in Figure 5, these changes are more prominently observed with TMIN and T2m than with TMAX, the two former series exhibiting always strong positive correlations (Figures 6a, 6b, and 6c).

[25] As underlined by *Collins* [2011], this long-term evolution is not predominantly a result of variations in ENSO. This is well illustrated in Figures 6a and 6b, which displays two TMAX peaks in Nino years (1983 and 1987) during the former period, then one peak in 1999 marked by a long and severe Nina event. By contrast, the temperature evolution is concomitant with SST evolution in the Northern Atlantic, and in particular of the positive phase of the AMO, but it can also be partially thought as an effect of changes in the North Atlantic Oscillation (NAO), since this atmospheric variability mode is known to exert impacts on thermal variability over the tropical Atlantic, the Mediterranean, and North Africa. In particular, Figure 1 of *Visbeck et al*. [2001] supports such a hypothesis, since it indicates that the positive (negative) NAO values are correlated with colder (warmer) winters in those regions. In fact, NAO series clearly shows that the index is more frequently positive in years 1980s and 1990s and more frequently negative after (http://www.cpc.ncep.noaa.gov/products/precip/CWlink/pna/JFM_season_nao_index.shtml). The interannual relationship in northern spring has been also verified through composite analyses over the March–May seasons, using the Jones NAO index [*Jones et al*., 1997] and the mean relative frequency of hot days over the period 1979–2011: it is 13.1% in negative NAO situations (Jones NAO < -1) and 6.9% in positive NAO situations (Jones NAO $> +1$), a difference statistically significant at $p = 0.05$.

[26] The greater frequency of heat waves occurrences with time can be also viewed as direct consequences of the greenhouse effect because it is more apparent in minimum temperatures registered at the end of the night than in diurnal maxima due to the less cooling of the accumulated diurnal energy during the night. However, this can be also due to increased surface humidity due to changes in the circulation, i.e., northward passage of the Intertropical Front [*Guichard et al*., 2009], low-level southerly anomalies associated with an intensified heat low in southern West Africa [*Knippertz and Fink*, 2008] or occurrence of tropical plumes [*Fröhlich et al*., 2013]. This will be discussed more in details in section 4.

[27] Table 2 displays the anomalies of Precipitable Water Content (PWT) and Specific Humidity (SHUM) at 2 m averaged over the Saharan (25°N–17.5°N) and Sahelian (17.5°N–10°N) zones inside the 10°W–10°E window. The results show that in March hot events are associated significantly with the water vapor content both at the surface and in the total atmospheric column, whereas in late spring and summer (June to August), one observes a clear decrease of

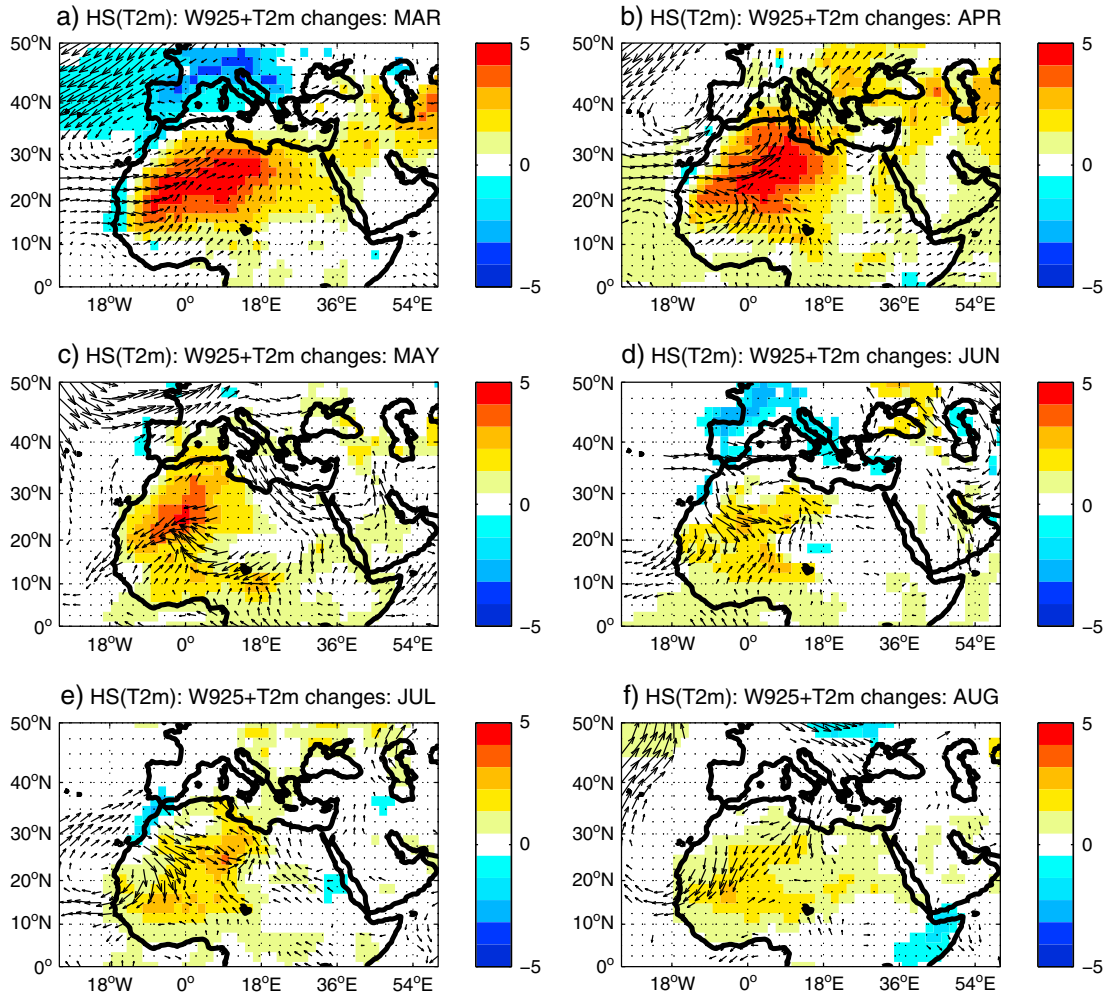

Figure 9. T2m (°C) and 925 hPa wind differences between days registering hot spells of at least 4 day long (using T2m90p threshold defined on 5 day moving windows) over 10°N–25°/10°W–10°E and all other days independently from the long-term evolution. The composite maps are displayed for the months of (a) March, (b) April, (c) May, (d) June, (e) July, and (f) August. For easy reading, only significant signals regarding a Student's *t* test at the 95% confidence level are displayed. Period 1979–2009.

these quantities (negative values in the three last columns of Table 2). Notice that such synoptic anomalies are opposed to the normal evolution of the mean seasonal cycle in terms of atmospheric moisture since they indicate more moisture in April and May and less from June to August.

[28] In order to better consider atmospheric conditions associated with successive days of abnormally warm temperature, anomalies in the daily air temperature, omega vertical velocity, and wind for hot day occurrences are now quantified within the tropospheric column over the region 10°N–25°N/10W–10E. Mean profiles are displayed in Figure 7 for all months from March to August for describing major features of the spring to summer evolution, while anomalies from the mean are displayed for the months of March, May, and July in Figure 8. They refer to the mean daily differences between hot events and all other days for a given month, and therefore must be interpreted on the basis of mean profiles in Figure 7. Comparison between Figures 7a and 7b and 8a–c shows that, from March to July, hot days are marked by a significant enhancement of the vertical temperature gradients due to increasing (decreasing) temperature under (above) the condensation level (~600 hPa). Figures 7c and 7d indicate maxima of air ascent at 850 hPa (negative values) and of air descent in midtroposphere increasing during the rainy season (Figure 7d). The enhancement of the vertical temperature gradients during hot days is associated with significant anomalies of air ascents (negative differences in omega) under the 500 hPa isobaric level (Figures 7c and 7d and 8b–d). For the months of May and July, one notices also increasing subsidence above this level (Figures 7c and 7d and 8e and 8f).

[29] Figures 7e–h and 8g–l illustrate the marked seasonal evolution of wind anomaly profiles during hot episodes. In March, one observes the existence of southwesterly anomalies under 850 hPa (positive zonal and meridional wind components in Figures 8g and 8j) attesting a vanishing of the mean Harmattan circulation by the end of northern winter (Figure 7). Similarly, in March and May, northeasterly anomalies occur in mid and high levels, indicating a weaker mean southwesterly flux (Figures 7e and 7g) and therefore a weaker subtropical westerly jet, the dominant feature at this altitude. In July, the existence of easterly and northerly anomalies in low levels (Figures 8i and 8l) identifies an

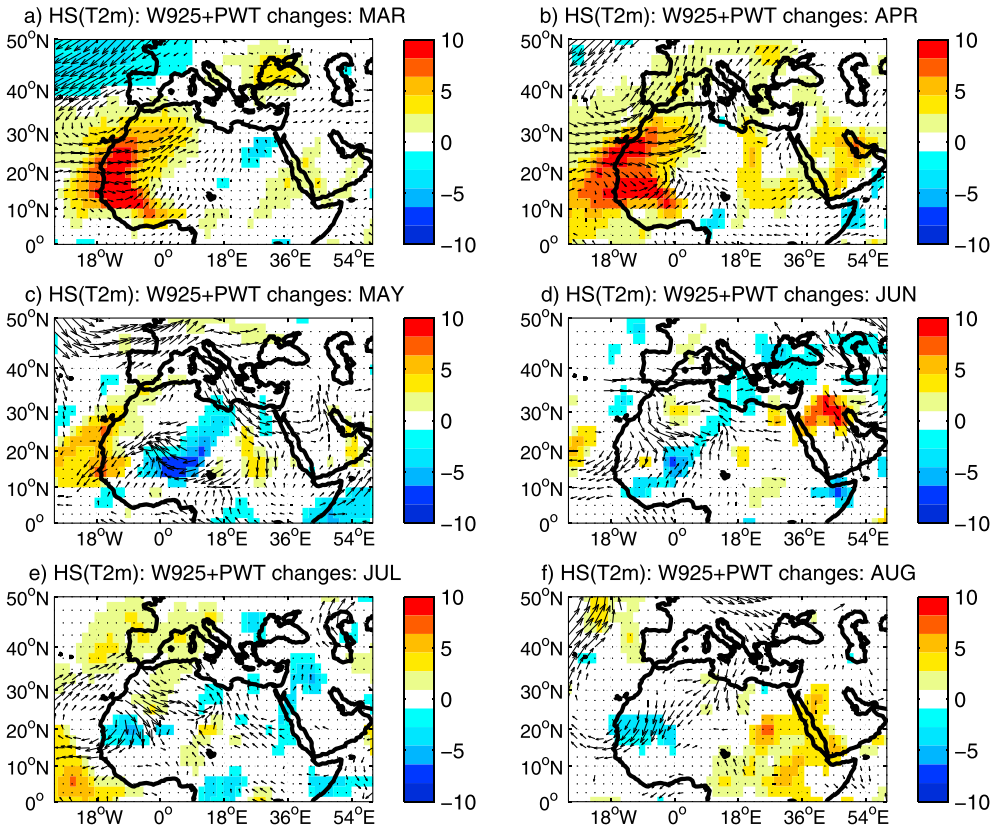

Figure 10. As Figure 9 except for the precipitable water content (g/m^2).

attenuation of the mean monsoon flow, while westerly anomalies in high levels (positive values in Figure 8i) point to a weaker TEJ.

[30] Thus, hot occurrences tend to be synchronous of wind anomalies opposed to the mean circulation in low levels, i.e., weaker Harmattan and subtropical westerly jet in winter and spring, weaker monsoon circulation and TEJ in summer. These anomalies of synoptic scale, in accordance with changes in PWT and specific humidity contents notified above (Table 2), tend therefore to be opposed to the mean seasonal cycle evolution. At the opposite, during summer, the northeasterly anomalies in midlevels (negative values in Figures 8i and 8l) indicate an enhancement and/or a northward displacement of the AEJ (Figure 7f). This is because hot occurrences in the 25°N–10°N belt tend to intensify surface warming there and therefore to make stronger the meridional thermal gradients driving the AEJ.

4. Associated Atmospheric Anomaly Patterns

4.1. Seasonal and Interannual Changes

[31] The results presented in previous sections document mainly the long-term trend. As a consequence, this tends to increase the occurrence of heat events by the end of the observation period. In order to complement the above approach, this section presents selected mean atmospheric anomaly fields associated with the T2m hot spells of at least 4 day long over the region 10°N–25°N/0°W–10°E. This choice is motivated by both the statistical and temporal distributions of heat wave duration already displayed in Figures 5 and 6, which show that the 4 day threshold is an efficient criterion.

[32] The results refer to the whole March–August period independently from the long-term 1979–2011 thermal evolution in low levels, described in section 3. This goal has been reached through the following steps:

[33] 1. T2m monthly means are defined at each grid point for each month (March to August) over the 33 years, for taking into account both the annual cycle and long-term evolution;

[34] 2. a low-pass butterworth filter is then applied on the monthly mean fields for eliminating the short interannual variability (< 3 years) and keeping only the multidecadal evolution of monthly means;

[35] 3. daily anomalies of a given month and year are then defined at each grid point by differencing each daily value from the filtered mean fields corresponding to this month and this year.

[36] Figures 9 and 10 present, respectively, the T2m (in Celsius) and PWT (kg/m^2) differences with the superimposed 925 hPa wind, while Figure 11 refers to the omega vertical velocity at 500 hPa (O500 in Pa/s) and the 600 hPa wind.

[37] Before the month of June, the highest T2m anomalies in HS occurrences are located over the western-central Sahara (Figures 9a–c). In March and April, and to a lesser extent in May, they are associated with a large cyclonic rotation anomaly lying off shore of Morocco in low and midlevels. Over the Ocean, this structure is associated with northerly anomalies reinforcing the mean flux in the eastern North Atlantic (Figures 9a and 9b and 11a and 11b), and over the continent with the presence of westerly and southwesterly anomalies from the Atlantic towards the Mediterranean. Over the Atlantic, trough occurrences significantly increase during low NAO situations, in particular during the March to May

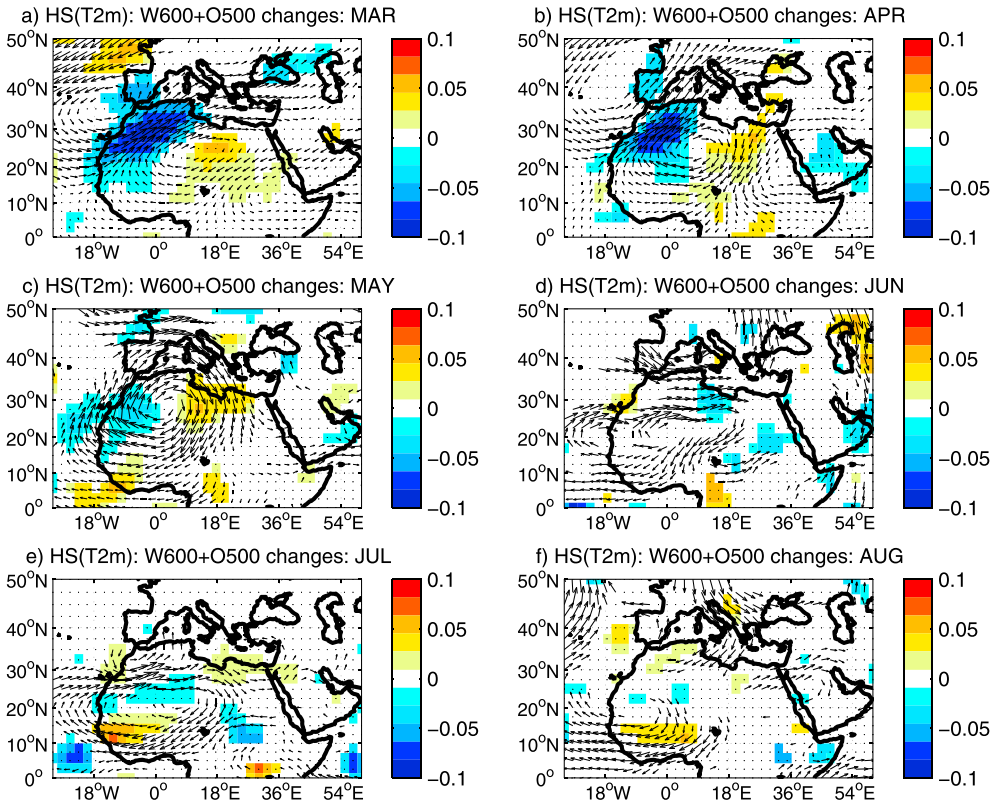

Figure 11. As Figure 9 but for the Omega vertical velocity at 500 hPa (dP/dz) and the 600 hPa wind.

season when troughs occur frequently. Thus, when a daily trough index is defined regarding the P10 percentile from the daily geopotential height at 1000 hPa averaged over the NW coast of Africa (25°N–45°N/25°W–10°W), the trough mean frequency is 16.5% in NAO− (Jones NAO < −1), and 7.3% in NAO+ (Jones NAO > +1), a difference statistically significant at $p = 0.05$.

[38] Over the continent, notice that the southerlies clearly reinforce in the Sahelian band in March to May (Figures 9a–c). Such signals are likely to lessen the mean Harmattan circulation over the Sahara. They are also linked to a clear dipolar PWT anomaly structure, enhancing PWT along the West coast and reducing PWT eastward to the 0° longitude (Figures 10a–c).

[39] The PWT increase over West Sahara is associated with negative O500 values in the midtroposphere (negative/positive in blue/red; Figure 11) associated with the trough circulation and indicating the existence of upward anomalies above a region of mean subtropical subsidence. By contrast eastward to the 0° longitude the subsidence reinforces in a region marked by an anticyclonic anomaly centered over central Sahara which tends to reinforce (weaken) the Harmattan flow over the eastern (western) Sahara and to reduce the dominant eastward circulation observed in March on the equatorward flank of the clockwise rotation (Figure 11a). These signals persist in April and May, although for 0500 decreasing westward and disappearing over central Sahara (Figures 11b and 11c).

[40] In this context, the month of June appears to be a transition month between winter-spring and summer configurations (panel d of Figures 9, 10, and 11). In northern summer, heat wave occurrences are dominated by the existence of a dominant flow from the North reducing the PWT content westward to 10°W and by southerlies reinforcing the monsoon flow eastward to 0° (Figures 9 and 10e–f). In August, enhanced northerlies from the Mediterranean favor the flux convergence with the monsoon flow over central and eastern Sahel, increasing locally the PWT content (Figure 11f). The 925 hPa northerlies in Figure 9 are linked to climatological Etesian winds blowing in summer over the eastern Mediterranean Sea as shown by *Gaetani et al.* [2010]. These winds tend to occur more often recently in connection with the significant warming of the Saharan and Mediterranean regions.

[41] In midlevels, by contrast, the anticyclonic anomaly located within the 20°N–30°N belt in spring persists in decreasing and migrating over the Western Sahara (Figures 11e–f). This reinforces the mean easterly circulation along the African Easterly Jet axis between 5°N and 10°N. The clockwise rotation is associated with three other signals: (i) easterly and southerly anomalies over the west coast, which favors a flux divergence on the northern flank of the AEJ over the Senegal; (ii) northerly anomalies eastward to the 0° longitude over the Sahara and Sahel intensifying the flow from the Mediterranean Sea; (iii) upward anomalies over central Sahara (negative values in blue shading and downward anomalies over the Sahel persisting in August (Figures 11e–f).

[42] All these maps demonstrate that atmospheric anomalies associated with the main heat waves are strongly coherent and well spatially defined although depending on the season considered. In particular, in spring when the mean temperature maximum is located between 10°N and 15°N (not shown), the enhanced southwesterly winds induce advection of higher temperatures north of 10°N and of moister air from the ocean,

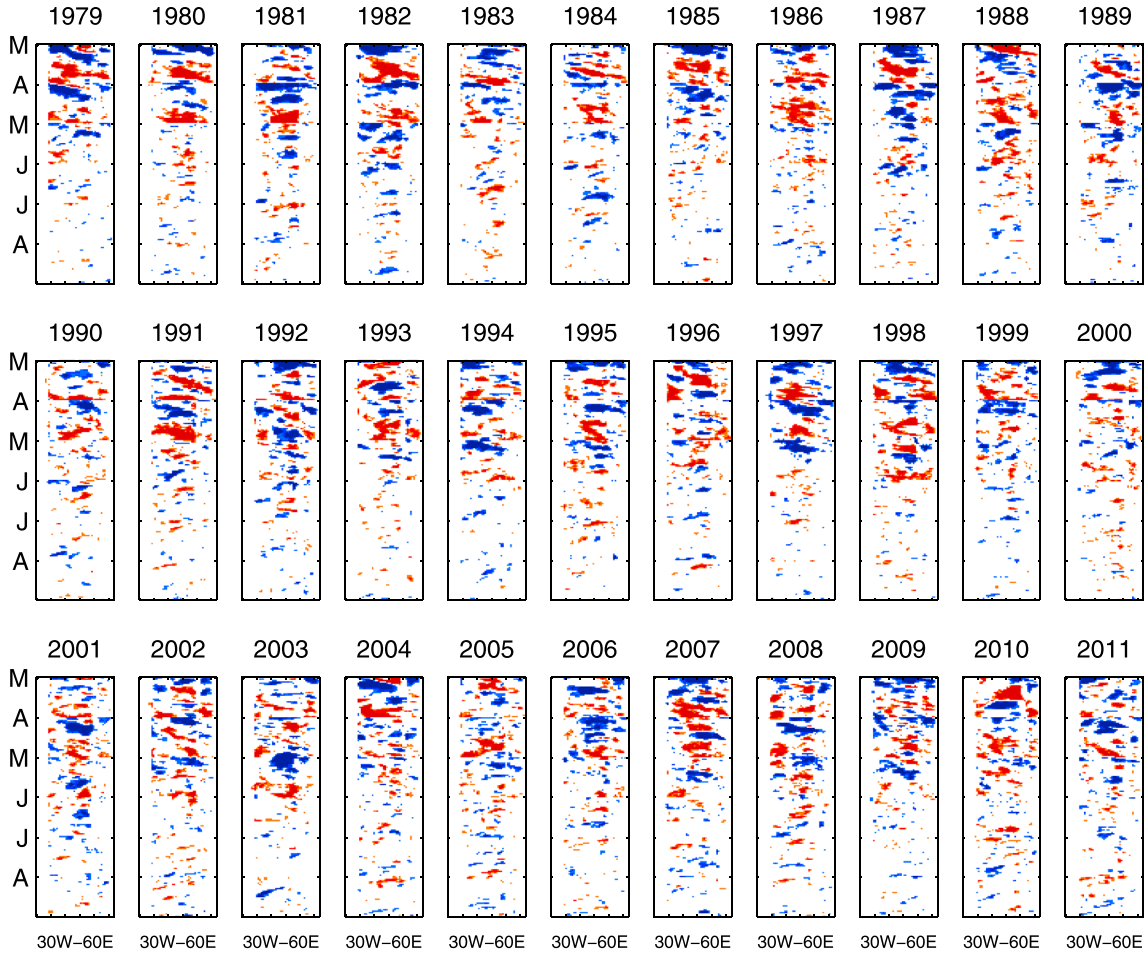

Figure 12. Longitude-time evolution of T2m anomalies averaged between 10°N and 25°N along the successive March to August seasons of the period 1979–2011. Only anomalies higher than 2°C in absolute value are displayed.

a circulation pattern highly favorable to heat wave occurrences. In Figures 5 and 6, the greater frequency of heat waves occurrences with time has been viewed in part as a direct consequence of the mean increasing greenhouse effect because it is more apparent in minimum temperatures registered at the end of the night than in diurnal maxima, due to the less cooling of the accumulated diurnal energy during the night by more greenhouse gas concentration (CO2 and water vapor). However, the local coupling between surface air temperature, atmospheric moisture content and radiative fluxes is not the sole element of explanation. We have shown that, independently of this long-term evolution, the synoptic scale atmospheric circulation clearly contributes to heat wave occurrences. The question of the potential link between the global warming and the long-term evolution of occurrence of the atmospheric pattern associated to these heat waves must be raised but it is out of the scope of this paper.

4.2. Zonal Propagation of T2m Anomalies and Synoptic Evolution Around Heat Waves

[43] The Hovmöeller diagrams in Figure 12 allow us to illustrate both the seasonal variability of significant T2m anomalies (> 2°C in absolute value) when averaged between 10°N and 25°N along with their zonal propagation from 30°W to 60°E over the 33 years. The panels confirm first that the March to May dry season is clearly more concerned by this type of event than the June to August rainy period, since about two to three main heat waves of at least 4 day length can be registered each year from March to May. Two other features appear: (i) in winter and spring, most thermal anomalies tend to propagate eastward from the African coast (~15°W) to about 60°E; (ii) after the end of May, the signals decrease both in intensity, duration, and zonal extent.

[44] So, in order to focus more on the mean synoptic evolution during the main seasons of heat waves, we concentrate on the period March–May in compositing atmospheric fields regarding heat waves occurrences of at least 4 day length over the period 1979–2011. Indeed, for comparing the resultant composite patterns and testing their robustness, several analyses with or without time filtering have been performed with different atmospheric variables and varying hot event durations (2 to 7 days) and time windows. It is noteworthy that the results obtained with these choices were in fact rather similar. Maps of Figures 13 and 14 can then be viewed as a good synthesis of all results. They present the time evolution of atmospheric anomalies in low and midlevels, along 8 day sequences centered on each heat wave of at least 4 day duration through five maps separated by 2 day intervals.

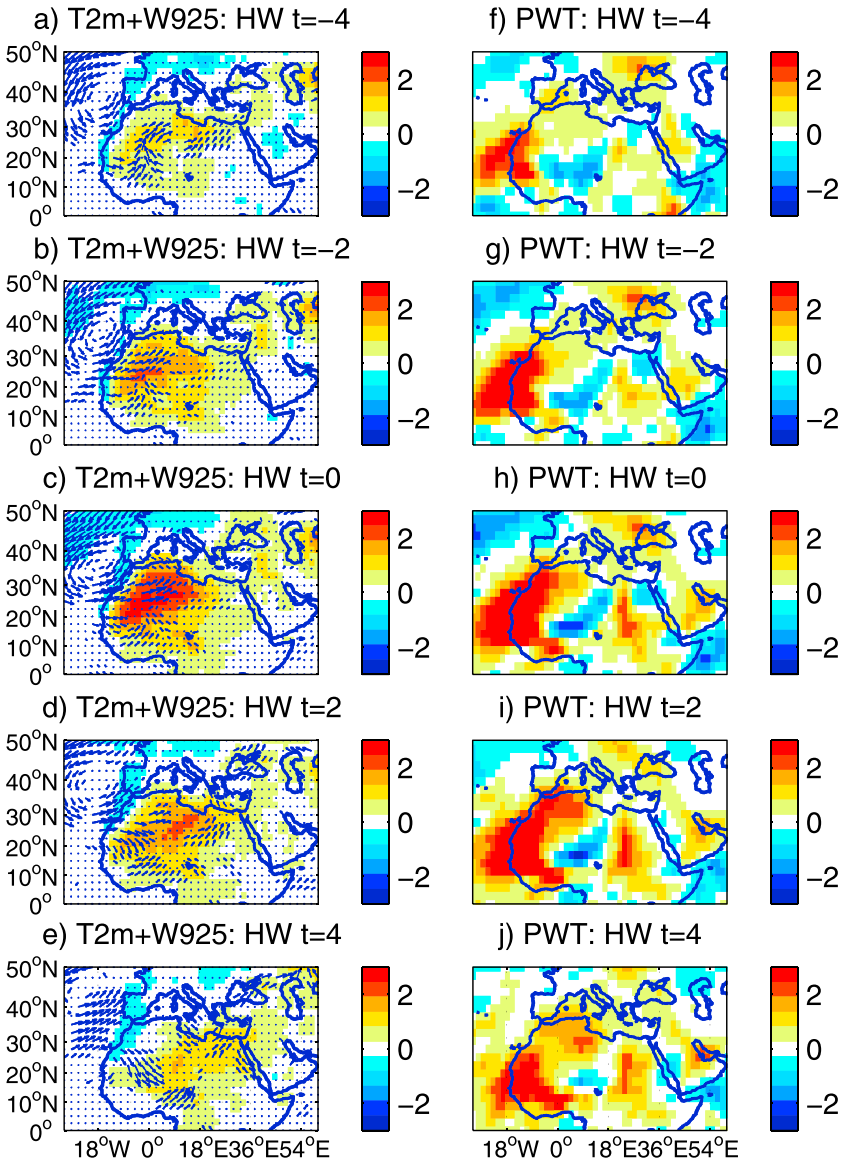

Figure 13. Tropospheric anomalies associated with heat waves of at least 4 day duration in March–May: (a–e) T2m (shadings in °C) and 925 hPa wind (vectors); (f–j) Precipitable water content in the atmospheric column (g/m^2). Period 1979–2009.

[45] For describing both the low and midtropospheric layers and keeping readability, Figures 13a–j document the air surface temperature at 2 m, the wind speed at 925 hPa and the precipitable water in the atmospheric column, while Figures 13a–j display the 600 hPa wind, the omega vertical velocity at 500 hPa, and the geopotential at 700 hPa.

[46] Before a heat episode, an abnormal warming of about 1.5°–2°C (yellow/red shading in Figures 13a and 13b) can be observed over the North of central Sahara and over the West-Central Sahara in association with southwesterly wind anomalies at 925 hPa. Synchronously, the PWT content increases over the west coast while it decreases over the central Sahel (Figures 13f and 13g). These features are concomitant with the installation of a dipolar zonal structure of O500 anomalies over Northern African coast and the Mediterranean, linked to an upward anomaly (Figures 14a and 14b, negative values in blue) westward to the warming area and by a downward anomaly eastward, over Libya and Egypt. This last feature reinforces locally the subtropical subsidence at 700 hPa (Z700) and generates an anticyclonic anomaly cell in the midtroposphere, as indicated, respectively, by the abrupt increase of geopotential height and wind rotation in Figures 14f and 14g. All these signals reach their maximum at t = 0 (Figures 13c and 13h; Figures 14c and 14h) then break up (Figures 13e and 13j; Figures 14e and 14j). It is seen also that air temperature and wind anomalies near the surface (Figures 13a–e), omega anomalies in the midtroposphere (Figures 14a–e) and to a lesser extent the subtropical subsidence and associated anomaly cell migrate eastward from the Atlantic to the Horn of Africa. These anomalies and zonal migrations are hence spatially coherent and particularly clear regarding the T2m and wind evolution at 925 hPa, along with the vertical velocity and wind patterns in midlevels. This suggests the role of short Rossby waves with an eastward

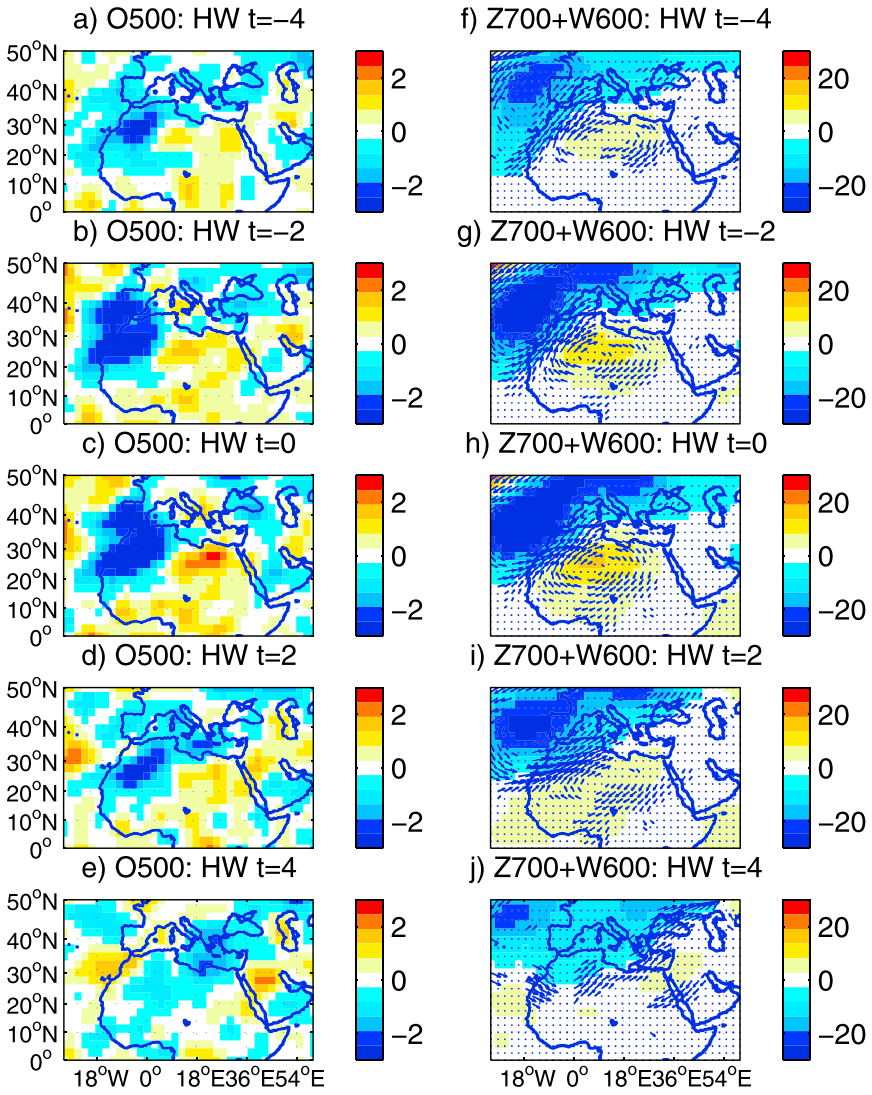

Figure 14. Tropospheric anomalies associated with heat waves of at least 4 day duration in March–May: (a–e) omega vertical velocity at 500 hPa (dP/dZ × 100); (f–j) 700 hPa geopotential (mgp × 10) and the 6010 hPa wind field (vectors). Period 1979–2009.

group velocity and a baroclinic mode possibly induced by the particular variability of the midlatitude atmospheric circulation and associated jet stream in winter and spring. This is supported by the Z700 anomalies (Figures 14f–j) indicating the presence in midtroposphere of a large trough with cyclonic vorticity over the Atlantic west of Europe and northern Africa.

5. Conclusion

[47] This study aimed at describing decadal evolution in air temperature and hot spell (heat waves) occurrences recently observed over the northern African continent in terms of magnitude, main location, annual cycle, and circulation changes in the troposphere.

[48] The results show that a clear and significant warming (1°–3°C) has been observed since the 1990s in all seasons over the whole region, after first appearing in northern spring by the mid-1960s over the continental Sahara and Sahel, eastward to the 0° longitude. The strongest warm anomalies follow with delay the course of the Sun. In March to June, they are located over the Sahel and Southern Sahara, mainly in the vicinity of the Saharan Heat Low but also on the eastern equatorial Atlantic, indicating unfavorable conditions for the cold tongue installation. In August, they lie over the Northern eastern Saharan, Arabian deserts, and western southern Europe.

[49] The current warming trend is associated after 1997 with (i) clear higher (lesser) frequency of warm (cold) daily mean and minimum temperatures, (ii) longer duration of heat waves in last years — shorter than 5 days before 1998 — and a mean frequency multiplied by 2 or 3 after, (iii) shorter day intervals between two consecutive events. Both former points are consistent with the highest occurrence of negative NAO in recent years. However, this can be also viewed as direct consequences of the greenhouse effect (less cooling of the accumulated diurnal energy during the night) since it is more apparent in minimum temperatures than in diurnal maxima, increased surface humidity, or changes in the circulation.

[50] Locally, warm episodes over the Sahara and Sahel are linked to wind anomalies opposed to the mean circulation in the high and low troposphere: weaker Harmattan and subtropical westerly jet in winter, increasing significantly the water vapor content both at the surface and in the total atmospheric column over West Africa; weaker southwesterly monsoon winds and TEJ in summer decreasing the atmospheric moisture content.

[51] Heat waves episodes have been examined over the period 1979–2011 after removing the long-term evolution. They are associated with specific atmospheric anomalies of larger scale depending on the season. From March to May, the highest T2m anomalies are located over the western Sahara and associated with a large low-level cyclonic rotation anomaly, lying over Morocco and reinforcing the mean flux in the eastern North Atlantic. This rotation lessens also the mean Harmattan circulation while atmospheric moisture contents augment (decrease) West (East) of the 0° longitude. In the midtroposphere, these signals are associated with upward (downward) anomalies above the western (eastern) subtropics, and an anticyclonic anomaly cell over central Sahara weakening (increasing) the Harmattan westward (eastward).

[52] In northern summer, heat wave occurrences are concomitant with a reduction of PWT content over the western regions of North Africa and of a cyclonic anomaly in central Sahel increasing locally the PWT content and flux convergence between the reinforced monsoon flow and northerlies from the Mediterranean. These northerlies, linked to climatological Etesian winds blowing in summer over the eastern Mediterranean Sea, tend to occur more often recently in connection with the warming observed over the Saharan and Mediterranean regions. South of the Sahara they tend to favor southward surges of hotter air of synoptic variability. In midlevels, by contrast, an anticyclonic anomaly locates over the Western Sahara. This reinforces both the African Easterly Jet and associated flux divergence over the Senegal and the northerlies anomalies from the Mediterranean eastward to the 0° longitude.

[53] The March to May dry season is clearly the most concerned by heat waves occurrences, with about two to three main events of at least 4 day length, propagating eastward. These events tend to be preceded by an abnormal warm episode, starting over Libya. They are associated with southwesterly anomalies over the West Sahara in low levels, and a reinforcement of subsidence and anticyclonic rotation in the midtroposphere. These anomaly patterns are spatially coherent regarding both the near-surface temperatures, the precipitable water content in the total atmospheric column and the omega and wind patterns in midlevels. In their built phase, they move slowly from the Atlantic and Maghreb to the central Sahara, then they disaggregate in migrating toward the Arabian Peninsula and Horn of Africa. Two other atmospheric features are also detected: a large trough structure concentrating cyclonic vorticity over the northern Atlantic, and an anticyclonic hot cell migrating from the central Sahara to the Arabian Peninsula. Such observations suggest the role of short Rossby waves with an eastward group velocity and a baroclinic mode possibly associated with jet stream deformation.

[54] This hypothesis needs more testing in terms of tropical-extratropical interactions in investigating the Weather Regimes over the Atlantic-Mediterranean-North African domain through atmospheric variables at the daily time scale, following the approach of *Polo et al.* [2011]. This will allow us to better quantify the potential impacts of some specific Weather Regimes, such as the North Atlantic Oscillation, to examine their persistence and transitions, as their links with heat waves configurations, recurrence, and statistics.

[55] Finally, the question of the potential link between the global warming and the long-term evolution of occurrence of the atmospheric pattern associated to these heat waves must be raised but it was out of the scope of this paper.

[56] **Acknowledgments.** The authors are grateful to the Climatic Research Unit (University of East Anglia), the National Oceanic and Atmospheric Administration (NOAA-CIRES ESRL/PSD Climate Diagnostics branch), the National Center for Atmospheric Research, and National Centers for Environmental Prediction for providing most of the data presented and the two anonymous reviewers for their interesting comments. The study was supported by the French component of AMMA. Calculations were performed using HPC resources from DSI-CCUB (Université de Bourgogne).

References

Aguilar, E., et al. (2009), Changes in temperature and precipitation extremes in western central Africa, Guinea Conakry, and Zimbabwe, 1955-2006, *J. Geophys. Res.*, *114*, D02115, doi:10.1029/2008JD011010.

Alexander, L. V., et al. (2006), Global observed changes in daily climate extremes of temperature and precipitation, *J. Geophys. Res.*, *111*, D05109, doi:10.1029/2005JD006290.

Arndt, D. S., M. O. Baringer, and M. R. Johnson (Eds) (2010), State of the Climate in 2009, *Bull. Am. Meteorol. Soc.*, *91*, S1–S224.

Chelliah, M., and G. D. Bell (2004), Tropical multidecadal and interannual climate variability in the NCEP–NCAR Reanalysis, *J. Clim.*, *17*, 1,777–1,803.

Christensen, J. H., et al. (2007), Regional climate projections, in *Climate Change 2007: The Physical Science Basis. Contribution of Working Group I to the Fourth Assessment Report of the Intergovernmental Panel on Climate Change*, edited by S. Solomon et al., 847–940, Cambridge Univ. Press, Cambridge, U. K.

Collins, J. M. (2011), Temperature variability over Africa, *J. Clim.*, *24*, 3649–3666.

Dunn, R. J. H., K. M. Willett, P. W. Thorne, E. V. Woolley, I. Durre, A. Dai, D. E. Parker, and R. S. Vose (2012), HadISD: A quality-controlled global synoptic report database for selected variables at long-term stations from 1973–2011, *Clim. Past*, *8*, 1649–1679, doi:10.5194/cp-8-1649-2012.

Fontaine, B., P. Roucou, M. Gaetani, and R. Marteau (2011a), Recent changes in precipitation, ITCZ convection and northern tropical circulation over North Africa (1979–2007), *Int. J. Climatol.*, *31*, 633–648, doi:10.1002/joc.2108, published online 10 March 2010.

Fontaine, B., P. Roucou, and P.-A. Monerie (2011b), Changes in the African monsoon region at medium-term time horizon using 12 AR4 coupled models under the A1b emissions scenario, *Atmos. Sci. Lett.*, *12*, 83–88, doi:10.1002/asl.321.

Fröhlich, L., P. Knippertz, A. Fink, and E. Hohberger (2013), An objective climatology of tropical plumes, *J. Clim.*, *26*, 5044–5060, doi:10.1175/JCLI-D-12-00351.1.

Gaetani, M., B. Fontaine, P. Roucou, and M. Baldi (2010), Influence of the Mediterranean Sea on the West African monsoon: Intraseasonal variability in numerical simulations, *J. Geophys. Res.*, *115*, D24115, doi:10.1029/2010JD014436.

Guichard, F., L. Kergoat, E. Mougin, F. Timouk, F. Baup, P. Hiernaux, and F. Lavenu (2009), Surface thermodynamics and radiative budget in the Sahelian Gourma: Seasonal and diurnal cycles, *J. Hydrol.*, *375*, 161–177, doi:10.1016/j.jhydrol.2008.09.007.

Harris, I., P. D. Jones, T. J. Osborn, and D. H. Lister (2013), Updated high-resolution grids of monthly climatic observations, *Int. J. Climatol.*, doi:10.1002/joc.3711, http://onlinelibrary.wiley.com/doi/10.1002/joc.3711/abstract, in press.

IPCC (2012), *Managing the Risks of Extreme Events and Disasters to Advance Climate Change Adaptation. A Special Report of Working Groups I and II of the Intergovernmental Panel on Climate Change*, edited by C. B. Field, et al., 582 pp., Cambridge University Press, Cambridge, UK, and New York, NY, USA.

Jones, P. D., T. Jonsson, and D. Wheeler (1997), Extension to the North Atlantic Oscillation using early instrumental pressure observations from Gibraltar and south-west Iceland, *Int. J. Climatol.*, *17*, 1433–1450.

Kalnay, E., et al. (1996), The NCEP/NCAR 40-Year Reanalysis Project, *Bull. Am. Meteorol. Soc.*, *77*, 437–471, doi:10.1175/1520-0477(1996)077<0437:TNYRP>2.0.CO;2.

Kanamitsu, M., W. Ebisuzaki, J. Woolen, S.-K. Yarg, J. J. Hnilo, M. Fiorino, and G. L. Potter (2002), NCEP-DOE AMIP-II reanalysis (R-2), *Bull. Am. Meteorol. Soc.*, *83*, 1631–1643.

Knippertz, P., and A. H. Fink (2008), Dry-season precipitation in tropical West Africa and its relation to forcing from the extratropics, *Mon. Weather Rev.*, *136*, 3579–3596, doi:10.1175/2008MWR2295.1.

Lavaysse, C., C. Flamant, S. Janicot, D. J. Parker, J.-P. Lafore, B. Sultan, and J. Pelon (2009), Seasonal evolution of the West African Heat Low: A climatological perspective, *Clim. Dyn.*, *33*, 312–330.

Lebel, T., and A. Ali (2009), Recent trends in the Central and Western Sahel rainfall regime (1990–2007), *J. Hydrol.*, *375*(1–2), 52–64, doi:10.1016/j.jhydrol.2008.11.030.

Meehl, G. A., C. Tebaldi, G. Walton, D. Easterling, and L. McDaniel (2009), Relative increase in record high maximum temperatures compared to record low minimum temperatures in the U.S., *Geophys. Res. Lett.*, *36*, L23701, doi:10.1029/2009GL040736.

Mitchell, T. D., and P. D. Jones (2005), An improved method of constructing a database of monthly climate observations and associated high-resolution grids, *Int. J. Climatol.*, *25*, 693–712, doi:10.1002/joc.1181.

Morak, S., G. C. Hegerl, and J. Kenyon (2011), Detectable regional changes in the number of warm nights, *Geophys. Res. Lett.*, *38*, L17703, doi:10.1029/2011GL048531.

New, M., et al. (2006), Evidence of trends in daily climate extremes over southern and west Africa, *J. Geophys. Res.*, *111*, D14102, doi:10.1029/2005JD006289.

Nicholson, S. (2005), On the question of the "recovery" of the rains in the West African Sahel, *J. Arid Environ.*, *63*(3), 615–641, doi:10.1016/j.jaridenv.2005.03.004.

Perkins, S., and L. Alexander (2012), On the measurement of heatwaves, *J. Clim.*, *26*, 4500–4517, doi:10.1175/JCLI-D-12-00383.1.

Peterson, T. C., P. A. Stott, and S. Herring (2012), Explaining extreme events of 2011 from a climate perspective, *Bull. Am. Meteorol. Soc.*, *93*, 1041–1067, doi:10.1175/BAMS-D-12-00021.1.

Polo, I., A. Ullmann, P. Roucou, and B. Fontaine (2011), Weather regimes in the Euro-Atlantic and Mediterranean sector and relationship with West African rainfall over the period 1989-2008 from a self-organizing maps approach, *J. Clim.*, *24*, 3423–3432, doi:10.1175/2011JCLI3622.1.

Santer, B. D., et al. (2007), Identification of human-induced changes in atmospheric moisture content, *Proc. Natl. Acad. Sci. U. S. A.*, *104*, 15,248–15,253.

Seneviratne, S. I., et al. (2012), Changes in climate extremes and their impacts on the natural physical environment, in *Managing the Risks of Extreme Events and Disasters to Advance Climate Change Adaptation*, edited by C. B. Field et al., *A Special Report of Working Groups I and II of the Intergovernmental Panel on Climate Change*, pp. 109–230, World Meteorological Organization, Geneva, Switzerland.

Trenberth, K. E., et al. (2007), Observations: Surface and atmospheric climate change, in *Climate Change 2007: The Physical Science Basis*, edited by S. Solomon et al., *Contribution of Working Group I to the Fourth Assessment Report of the Intergovernmental Panel on Climate Change*, pp. 235–336, Cambridge University Press Cambridge, United Kingdom and New York, NY, USA.

Visbeck, M. H., J. W. Hurrell, L. Polvani, and H. M. Cullen (2001), The North Atlantic Oscillation: Past, present, and future, *Proc. Natl. Acad. Sci. U. S. A.*, *98*(23), 12,876–12,877, Epub 2001 Oct 30.

Willett, K. M., P. D. Jones, N. P. Gillett, and P. W. Thorne (2007), Attribution of observed surface humidity changes to human influence, *Nature*, *449*, 710–712, doi:10.1038/nature06207.